How “hot” are hotspots: Statistically localizing the high-activity areas on soil and rhizosphere images

Nataliya Bilyera[a,b,], Irina Kuzyakova[c], Andrey Guber[d], Bahar S. Razavi[a], Yakov Kuzyakov[e]*

a – Dept. Soil and Plant Microbiome, Institute of Phytopathology, Christian-Albrechts-University of Kiel, 24118 Kiel, Germany

b – Dept. of Soil Science, Institute of Soil Science and Plant Nutrition, Christian-Albrechts-University of Kiel, 24118 Kiel, Germany

c – Dept. Ecoinformatics, Biometrics and Forest Growth, University of Göttingen, 37077, Göttingen, Germany

d – Soil, Plant and Microbial Sciences, Michigan State University, East Lansing, MI 48824, USA

e – Dept. of Agricultural Soil Science, Dept. of Soil Science of Temperate Ecosystems, University of Göttingen, 37077, Göttingen, Germany

* corresponding author

E-mail address: nbilyera@yahoo.com (Nataliya Bilyera)

Abstract

The recently raised topic of microbial hotspots in soil requires not only visualizing their spatial distribution and biochemical analyses, but also statistical approaches to identify these hotspots and separate them from the surrounding activities (background). We hypothesized that each type of hotspot (e.g. microbial hotspots of enzyme activities, (bio)chemical hotspots of root exudation, herbicide accumulation) is a result of local processes driven by biotic and/or abiotic factors, and the rates of such processes in the hotspots are much higher than those in the general background. We further hypothesized that the background activities in soil are normally distributed. Consequently, hotspot determination should be based on statistical separation of activities significantly higher than the background. We used three groups of published images: 1) ^{14}C images of carbon input by roots into the rhizosphere, 2) ^{14}C glyphosate accumulation in the plant, and 3) soil zymogram of leucine aminopeptidase activity in soil. Each image was analyzed for the statistical distribution of grey values. The two Gaussian distributions were fit (the first representing the background, the second the hotspots) to the distribution of grey values in the images, the parameters (means and standard deviations, SD) of the fitted distributions were calculated, and the background was removed. For the parameters with one distribution, we identified hotspots as areas outside of the Mean+2SD image intensity (corresponding to the upper ~ 2.5% of activity, being over 97.5% of background values). Finally, we visualized images of solely hotspot locations. We compared the results with previously used decisions on hotspot intensity thresholding (i.e. Top-25%, as well as 17 standard thresholding approaches in ImageJ) and then presented and discussed the advantages of the Mean+2SD approach. These advantages include: i) unification of the thresholding approach for several imaging methods with various principles of activity distribution, ii) identification of hotspots with various activity levels, iii) analysis of "time-specific" hotspots in temporal sequences of images. We compared this with 17 standard thresholding methods and conclude that objectively elucidating and separating the

hotspots, e.g. using the Mean+2SD or Mean+3SD approach, should be based on statistical tools of distribution analysis. This approach helps to understand the processes responsible for the highest activities.

Keywords: Microbial hotspots quantification, Statistical analyses, Rhizosphere, Visualization approaches.

1. Introduction

Soil imaging methods have developed rapidly in recent decades with the advent of advanced techniques (Protz et al., 1987). Various non-destructive methods enable visualizing and quantifying parameters reflecting root-soil-microbial interactions (Oburger and Schmidt, 2016). The non-destructive methods yield soil images at a broad range of scales starting from a few nm (10^{-9} m) up to meters (>1 m) (Schlüter et al., 2014). These methods reliably identify the location and spatial distribution of hidden soil life. They are based on a very broad range of approaches: 1) soil zymography: visualization of enzymatic activity in soil (Spohn et al., 2013), rhizosphere (Razavi et al., 2019, 2016), detritusphere (Liu et al., 2017) and earthworm burrows (Hoang et al., 2016); 2) autoradiography and radioisotope imaging: localization of root exudation patterns (Holz et al., 2018) or pesticide accumulations (Alcántara-de la Cruz et al., 2016; Nandula and Vencill, 2015; Pereira et al., 2019) in plants and soil; 3) neutron imaging of water distribution (Carminati et al., 2010); 4) hyperspectral imaging for quantitative soil classification (Steffens and Buddenbaum, 2013); 5) spatial distribution of SOM fractions by reflectance (Steffens et al., 2014); 6) nano-scale secondary ion mass spectroscopy (nanoSIMS) for nano-scale element heterogeneity and speciation (Werner et al., 2017). Other *in situ* imaging approaches are described in detail in Oburger and Schmidt (2016).

Spatial visualization is essential for characterizing and quantifying hotspot processes. Such quantification includes (but is not limited to) the following directions: 1) the principles of hotspot localization: frequency, distribution, common distances and size – the spatial pattern; 2) thresholding by process intensities; 3) connection between microbial hotspots and the physicochemical conditions: co-localization of images for various parameters; and 4) clear separation of the hotspots from the background.

72 The ***first direction*** was successfully developed based on the geostatistical analysis and
73 spatial point pattern analysis of microbial distributions in soil in 2-D (Nunan et al., 2002, 2001)
74 and 3-D space (Kravchenko et al., 2013; Nunan et al., 2003).
75 Various approaches related to the ***second direction*** have been recently developed for the
76 hotspots identified using soil zymography. These include thresholding of the Top-25% grey
77 value intensities (Ma et al., 2017), over 20% (Zhang et al., 2019), 50% (Heitkötter and
78 Marschner, 2018) or 70% (Liu et al., 2017) of mean grey value, and the percentage of
79 segmented areas with the highest enzyme activity that were calculated after determining
80 them as hotspots (Spohn and Kuzyakov, 2014).
81 The development of correlative imaging (Handschuh et al., 2013; Polzer et al., 2019)
82 successfully advanced the ***third direction***. Combining 3-D (X-ray) with 2-D light and
83 fluorescent microscopy, SIMs and NanoSIMs methods revealed that about ¾ of
84 microorganisms preferably occupy soil micropores <10 μm (Schlüter et al., 2014) or pores <
85 100 μm (Kravchenko et al., 2019b). The 3-D pore size distributions and particulate organic
86 matter determined by X-ray μCT was correlated with enzyme-active locations identified on
87 multiple 2-D soil cross-sections to identify the locations of soil carbon stabilization
88 (Kravchenko et al., 2019b).
89 The present methodological study belongs to the ***4th direction*** and is designed to localize the
90 hotspots based on contrasting image intensities with the background.
91 In a recent review, Roose et al. (2016) strongly supported the statistical tools for objective
92 image interpretation. Such tools, including variation indexes (Lv et al., 2019), multiple-linear
93 regression (Qiu et al., 2003), and linear and non-liner models (Zhu et al., 2017), were
94 successfully applied for hotspot detection (Table 1). Imaging protocols in neuroscience were
95 developed by using statistical approaches (Dinov, 2011) based on parametric (e.g., paired *t*-
96 test, Two-way ANOVA) and nonparametric (e.g. Kruskal-Wallis, Fliegner-Killeen) statistical
97 tests (Chu et al., 2009) or spatial mixture models (Logan et al., 2008). *K*-means cluster

98 statistical analysis was applied to define phosphorus-rich regions imaged using NanoSIMs
99 (Werner et al., 2017) and SIMs (Bertrand et al., 2001) in soil (Table 1). One-way analysis of
100 variance (ANOVA) was applied to find the boundaries between low and medium activities and
101 the borders of hotspots visualized by soil zymography (Ge et al., 2017; Hoang et al., 2016).
102 ANOVA approach was based on comparing mean values for 4 adjacent pixels and applicable
103 to contrast zones (i.e. rhizosphere, detritusphere, biopores). Unfortunately, the approach was
104 unreliable in low-contrast areas on images. Applying ANOVA is not entirely suitable for
105 imaging methods when the activity at two adjacent pixels is interdependent, or when the
106 prerequisites (independent observations, normal distribution, variance homogeneity) for
107 ANOVA are not fulfilled.
108 Microbial hotspots have been defined as small soil patches with considerably higher process
109 rates than those within the bulk soil (Kuzyakov and Blagodatskaya, 2015). No standardized
110 statistical approaches are currently available for thresholding hotspots in soil imaging
111 applications. This study picks up the challenge and develops and tests a simple approach to
112 identify hotspots in the bulk soil.
113 We hypothesize that a sharp gradient is present between hotspots and background activity
114 (e.g., enzyme activity in the rhizosphere and bulk soil). Thus, if the background activity in the
115 bulk soil follows the normal distribution, then activities above the Mean + 2 standard
116 deviations (SD) (Mean+2SD) are hotspot related.
117 To separate the distribution of the probability of hotspot locations from the background and to
118 set a threshold, we suggest the Mean+2SD approach. This approach enables obtaining an
119 error probability of < 2.28% (half of all values outside of the ± 2 SD covering 95.44% of all
120 values within the normal distribution). Consequently, if the hotspot area exceeds 2.28%
121 (which corresponds to the normal distribution), then there are specific reasons and processes
122 for the origin of the area with the highest image intensities – the hotspots. According to these

prerequisites, the statistical definition of hotspots would be: Hotspots are those soil volumes in which the activities of the studied process exceed 2 SD of the mean in bulk soil.

2. Materials and methods

2.1. Images for statistical analysis of hotspots

Three groups of images representing hotspots of different origin were taken from literature: 1) spatial distribution of leucine aminopeptidase activity on soil zymogram (Razavi et al., 2017); 2) spatial distribution of ^{14}C labeled glyphosate in plants (Pereira et al., 2019), and 3) ^{14}C allocation in living roots and exudates (Holz et al., 2018).

All images were processed using the open source software ImageJ (Schindelin et al., 2012). To avoid detailed descriptions of all the underlying experiments elsewhere and to help restrict the data solely to own studies, we have chosen the digital images presented in already published papers (see below). Only the original images (untreated and uncorrected) – monochrome (^{14}C autoradiograms) or taken under UV light (zymograms) – were used; none of these images was transformed by the authors of original papers to color images. The color images (Red-Green-Blue, RGB) usually used in papers for better visualization were excluded because the blue and red colors corresponding to low and high values of a particular parameter are commonly adjusted by the authors and may not be proportional to the grey intensities in the original image. Thus, although color pictures are better for visualization and presentation in publications, they are not suitable for statistical analysis and can cause incorrect data interpretation. The monochrome digital images were converted to 8-bit greyscale images and inversed, if necessary, to obtain lowest value for 0 and the highest greyscale value for 255.

2.2. Mean + 2SD methodology for hotspot thresholding

Determining hotspots in each image involved 3 steps: 1) splitting the greyscale histogram of the image to two histograms with normal distribution of greyscale values; 2) identifying the greyscale range corresponding to the hotspots; and 3) hotspot mapping on the original image.

1st step: Splitting the greyscale histogram. The intensity of grey values and the corresponding number of pixel counts on images (histograms) were calculated using Histogram toolbox of ImageJ. Statistical analyses were conducted in R, version 3.5.1 (R Developement Core Team, 2014). The package "mixtools" (Benaglia et al., 2009) was used for distribution fitting. The parameters of normal distribution were fitted to the original frequencies of grey values (0…255). Then, the modeled distributions were built and plotted as a histogram (Fig. S1). The *normalmixEM* function in the "mixtools" package based on the expectation–maximization (EM) algorithm was used to fit two Gaussian component densities to the histogram of grey value intensities. The following characteristics of the two normal distributions were identified and calculated (Figs. 1 and S1): **lambda** (λ) corresponds to the share of each distribution component in the total area occupied by grey values of all activities in the whole histogram, **mu** (μ) corresponds to the mean value, and **sigma** (σ) corresponds to the standard deviation (SD) of each histogram (Fig. S1).

2d step: Identifying the greyscale range corresponding to the hotspots. The component with the lower mean value was chosen as a background distribution, representing the bulk soil, while the component with the higher mean value represented the hotspots. Because of considerable overlapping of the two components of the original greyscale histogram (Fig. S1), any single-value thresholding method attributes part of the overlapped area either to the background or to the hotspots. In our approach, we consider hotspots to be represented by pixels with grey values greater than Mean+2SD of the background component of the

greyscale histogram. Therefore, to remove 97.5% of the background, the sum of the Mean+2SD was used as a threshold for the original image histogram.

3^{d} step: Hotspot mapping on the original image. Hotspot percentage was calculated, and solely hotspots were mapped in red on the original images by setting a threshold value using the open source software ImageJ, clearly visualizing these locations.

Tested images had two background origins: i) enzyme activity of bulk soil on the zymogram (Fig. 2) and ^{14}C image of labeled roots and exudates (Fig. 3); and ii) background activity (noise) on the plate – in the ^{14}C image for glyphosate content in plants (Fig. 4). Therefore, we applied the parameters (mean and SD) of the component 1 (representing the background) (Fig. S1) to threshold hotspots in soil (Figs. 2 and 3). Three components were present on the plant image labeled with ^{14}C glyphosate. Specifically, the background around the plant (component 1), plant without glyphosate (component 2) and plant with glyphosate (component 3, i.e. hotspot). To identify the hotspots in the plant, we used the parameters of component 2 (Fig. S1) to threshold hotspots in the scanned plant (Fig. 4).

The hotspot area and hotspot localization for the presented Mean+2SD and Mean+3SD statistical approaches were compared with the results obtained by the frequently used Top-25% approach (Ma et al., 2017). The Top-25% hotspot approach is based on the thresholding grey values (i.e. enzyme activity in soil zymography) in the upper quartile (Top 25%) (Ma et al., 2017). The Mean+3SD approach is similar to Mean+2SD, but enables separating the hottest spots (0.15%) by thresholding 99.85% of the background values.

2.3 Comparison with standard thresholding methods

To compare hotspots defined by the proposed Mean+2SD approach with those defined by traditionally used thresholding methods, we applied 17 thresholding methods built-in in ImageJ software: Default, Otsu, Huang, Triangle, Lee, Mean, MinEntropy, Minimum,

194 Percentile, MinError, Shanbhag, IsoData, IJ_IsoData, Moments, Intermodes, RenyiEntropy,
195 Yen (see details in Landini, 2017, ImageJ, ver. 1.16.5). Since the original images were
196 published in 8-bit format (i.e. greyscale values ranged from 0 to 254), the activities in hotspots
197 were compared in relative units (0-1). The thresholding of the ^{14}C image of glyphosate
198 distribution in the plant was applied to the plant area to exclude the effect of the background
199 around the plant on the hotspot detection. The thresholding of the soil zymogram and ^{14}C-
200 labeled roots was applied to the whole images. The normalized activities and relative area of
201 the hotspots calculated using the standard thresholding methods and Top-25% approach
202 were compared with the results of Mean+2SD and Mean+3SD thresholding.

203

204 3. Results

205 3.1. Mean+2SD and Mean+ 3SD vs. Top-25% thresholding

206 Application of the Mean+2SD and Mean+3SD approaches enabled identifying the hotspots of
207 enzyme activity on the leucine aminopeptidase zymogram as being 12% and 7.1% of the
208 image area, respectively (Fig. 2). The hotspots were identified by these statistical approaches
209 mainly along the roots (rhizosphere hotspots) and in the root-free zones (microbial hotspots).
210 Mean+2SD yielded 5% more hotspot area than Mean+3SD because of extended rhizosphere
211 size and due to more micro-hotspots located in the bulk soil (Fig. 2). In contrast, the Top-25%
212 approach thresholded only 0.2 % as a hotspot located in the most active regions of roots.
213 Thus, Mean+2SD and Mean+3SD approaches thresholded 60 and 36 times larger hotspot
214 area for leucine aminopeptidase activity (Fig. 2, Table 2) than the Top-25% approach.

215 The difference between hotspot areas for the newly tested statistical approaches and Top-
216 25% for the ^{14}C content in soil and exudates (Fig. 3) was much lower that for soil zymography

(Fig. 2). The total hotspot areas for ^{14}C in root exudates and roots (Table 2, Fig. 2) were about 4 and 3 times larger for the Mean+2SD and Mean+3SD approaches, respectively, than Top-25%.

The hotspot areas thresholded by the Mean+2SD and Mean+3SD approaches for image of ^{14}C glyphosate content in plant were 4.6 and 2.6 times larger than Top-25% (Table 2). Furthermore, hotspots thresholded by Top-25% and Mean+3SD were located in seed but not in the leaves, whereas Mean+2SD detected hotspots in both plant components (Fig. 4). Thus, mapping hotspots thresholded by three approaches – Mean+2SD, Mean+3SD and Top-25% – revealed significant visual and quantitative differences in hotspot features (Figs. 2-4). These differences include: i) the total area covered by the hotspots and ii) the localization pattern.

3.2. Comparison of suggested approach with standard thresholding methods

The performance of the standard ImageJ thresholding methods differed for three tested images. The smallest hotspot area was obtained for the soil zymogram using Minimum method, while the largest was obtained using Percentile method. The difference between the smallest and largest areas estimated by the standard methods was 500 times (Fig. 5a). The ranks of the standard methods changed, though the difference between Minimum and Percentile methods was still 12-fold when thresholding was applied to the $^{14}CO_2$-labeled root image (Fig. 5b). The differences between standard methods were even more pronounced for the ^{14}C-labeled glyphosate image (Fig. 5c), reaching about 1600 times between Shanghang and Percentile. Changing ranks of the standard methods indicated overall inconsistency in their performance for detecting hotspots. Persistently intermediate values of the hotspot area were obtained using the Mean+2SD and Mean+3SD approaches for the first two tested images and close to mean for the cluster of 7 standard methods for the third image, indicating

241 robustness of the developed approach. As expected, normalized mean hotspot activities
242 (from 0 to 1) computed by different standard method but for the same images demonstrated a
243 trend opposite to that for hotspot areas. Smaller average activities were observed for those
244 segmentation methods that produced larger hotspot areas (Fig. 6). Similar to the hotspots,
245 the Mean+2SD and Mean+3SD approaches generated intermediate estimates of the mean
246 hotspot activity (except for ^{14}C-labeled glyphosate in plants, which showed intermediate
247 estimates only for the cluster of 7 standard methods) among the tested methods.

248 4. Discussion

249 4.1. Why statistical methods are necessary for hotspot thresholding

250 For the first time in 2-D soil imaging, we suggest using a simple and freely available statistical
251 approach to detect and localize microbial hotspots. The approach based solely on separating
252 statistical distributions for the background and hotspots is important for quantitatively
253 assessing hotspot areas and localizing them. Separation based on intensity level (but
254 ignoring the density of each pixel (Fig. S1)) may either under- or overestimate hotspot areas,
255 leading to misinterpretation of *in situ* soil processes and activities. All three examples (Figs. 2-
256 4, Table 2) showed underestimation of hotspot areas by the frequently used Top-25%
257 compared to the suggested Mean+2SD approach. We conclude that the main reason for this
258 underestimation by Top-25% is inherent in the nature of the approach: the Top-25% is
259 defined by few “hottest” points (Fig. 1) and, in an extreme case, by only one point with
260 maximal activity, thus making it always strongly biased to the right on the activity distribution
261 (Fig. 1). As the whole range of pixel intensities will be divided into four quartiles (25% in
262 each), any points below Top-25% will be automatically disregarded as hotspots, even if they
263 differ significantly from the normal distribution of the background. On the example of the
264 distribution of the pixel grey scale (corresponding to intensities, Figs. 1, S1) on the 8-bit

265 image, all points below grey intensity 192 will be disregarded as hotspots using the Top-25%
266 approach. In contrast, the Mean+2SD approach will definitely highlight these hotspots,
267 including those that are much closer to the background (Figs. 1 and S1).
268 The distributions of pixel intensities on 2-D soil images are generally bimodal, i.e. two-class
269 pictures consisting of background and hotspots. The main task of thresholding is to determine
270 the objective reasons and threshold value to separate the pixels with high and low intensities
271 (light from dark on the images). Various statistical approaches have already been suggested
272 in soil hydrology (Lv et al., 2019; Qiu et al., 2003; Zhu et al., 2017), but being technique-
273 specific, they cannot be applied directly to all image types (Aslantas et al., 2017).
274 In a pioneering study on image processing, the mean and standard deviations for peaks of
275 grey-value classes were applied for cell types separation corresponding to various grey-value
276 classes (Prewitt and Mendelsohn, 1966). Mean and standard deviations are the parameters
277 of the well-established Otsu (1979) thresholding approach, which has been used widely for
278 40 years in medicine and biology based on its clarity and simplicity. That approach is being
279 used as a basic technique for distinguishing between cell compartments on various images.
280 Since that time, various other thresholding approaches (mostly used in diagnostic imaging in
281 medicine) have been developed (Aslantas et al., 2017; Lee et al., 1990; Matsuyama et al.,
282 2016) and became available in imaging software. Triangle (Zack et al., 1977) has a good
283 potential for separating rhizosphere hotspots because it was successfully applied for root
284 thresholding (Tajima and Kato, 2013, 2011). The thresholded hotspot areas by triangle
285 method were similar to Mean+3SD approach showing highest p-value (Table S1) for an
286 image of leucine aminopeptidase distribution along the roots (Fig. 5 a). The Huang method
287 (Huang and Wang, 1995) produced the exact same hotspot area and mean value (*p=1*, Table
288 S1) as the Mean+2SD approach on the ^{14}C image for root and exudates in soil. None of the
289 17 auto thresholding methods (Figs. S3, Table S1) yielded the results very close to
290 Mean+2SD (Fig. 5 a-c) on the ^{14}C image of ^{14}C-labeled glyphosate in plant. Moreover, Yen,

291 ReniyEntropy and MaxEntropy were not statistically different from Mean+3SD (Table S1) and
292 revealed similar results for hotspot areas. Therefore, Yen, Triangle, Huang, ReniyEntropy and
293 MaxEntropy methods in ImageJ have a very good potential to threshold microbial and
294 (bio)chemical hotspots on soil images. Nonetheless, further studies are needed to test these
295 thresholding methods on a broad dataset of soil images.

296 *4.2. Comparison of the Mean+2SD, Mean+3SD and Top-25% approaches*

297 Applying the Mean+2SD and Mean+3SD approaches for hotspot separation on soil
298 zymograms revealed an up to 36-60 times larger area than the Top-25% approach and
299 helped better localize root and rhizosphere zones on hotspot images(Figs. 2-4, Table 2).
300 Following the statement about the rhizosphere being a microbial hotspot (Kuzyakov and
301 Razavi, 2019), it is evident that hotspots are localized along the whole root system (Fig. 2)
302 and not restricted to the very few root regions revealed by Top-25% thresholding. Clearly, the
303 Mean+3SD approach thresholded fewer roots within hotspots than Mean+2SD and should
304 therefore be applied with caution in rhizosphere studies.

305 In contrast to the soil zymogram, the difference for hotspot areas on ^{14}C images evaluated by
306 the three approaches (Mean+2SD and Mean+3SD vs. Top 25%) was much lower (but still
307 very high – from 2.4 to 4 times) or negligible (< 0.1 %) (Fig. 4 a-b). We explain this lower
308 difference by the specifics of the ^{14}C imaging method and its processing: i) usually, ^{14}C
309 images have a higher contrast than zymograms (for some uncertainties and constraints of ^{14}C
310 images, see Holz et al. (2019)); this higher contrast reflects the absence of ^{14}C activity in the
311 background soil (the radiocarbon or bomb ^{14}C can be disregarded compared to ^{14}C labeling;
312 the same is valid for cosmogenic or geogenic radioisotopes); ii) ^{14}C images contain many
313 pixels at the maximal grey value of 255, which is not relevant for zymograms. These highest

values are definitely thresholded by all three approaches (Mean+2SD, Mean+3SD vs. Top 25%) on ^{14}C images.

In contrast to enzyme activities on soil zymograms, the ^{14}C footprint on images is localized along the roots in soil and in most cases mimics root shape very well (Fig. 4 a-b). Therefore, shape-based methods for segmenting such ^{14}C exudation hotspots (Gao et al., 2019) can be an option for further thresholding improvement. Note, however, that object-based segmentation is inapplicable for soil zymography due to the location of micro-hotspots in micropores (Kravchenko et al., 2019a) and due to the large variation of individual areas from 0.00034 to 2.8 mm^2 (Guber et al., 2018). To avoid any bias, we recommend the pixel-based method for evenly distributed (not object-based) enzyme activity in bulk soil. For details on the advantages and disadvantages of pixel-based and object-based analysis, see the review of Hussain et al. (2013) .

4.3. Limitations of statistical approaches to distinguish and localize hotspots

Hotspot thresholding by statistical approaches based on the distribution of pixel intensities has a great advantage because it is person-independent and enables a unified analysis of the obtained images. Nonetheless, certain shortcomings – which are actually independent of the used statistical approach – need to be considered.

1) The quality of the original images plays a significant role in precise hotspot determination. Thus, a **low signal-to-noise ratio** likely results in a wider Gaussian distribution (Weszka and Rosenfeld, 1978) and, consequently, larger SD value. Therefore, poor-quality original images leads to a decrease in some hotspot areas, and some hotspots can even disappear completely. This problem is relevant for any thresholding approach. Solving this issue in image analysis requires: i) improving the quality of the original experimental images, and ii) avoiding the smoothing or de-noising of the original image. This second option may lead to

losses of some small hotspots (e.g. in micropores with Ø=60-180 µm (Kravchenko et al., 2019a)) or decreases in hotspot areas.

2) The complexity of soil life and processes can yield a **few (more than two) distributions** of grey values, each reflecting individual process groups or substance concentrations. Each of these distributions reflects specific reasons or mechanisms. We assume that the first distribution (on the left in Fig. 1) always belongs to the background, and further possible distributions represent hotspot groups caused by various factors. Each hotspot area (peak in the intensity distribution) can be segmented by applying the same procedure further and assuming the next distribution as a background for the remaining hotspots. Thus, evaluating hotspots originating by various processes requires moving toward multi-level thresholding (Mortazavi et al., 2012; Satapathy et al., 2018).

3) It is difficult to **distinguish between** hotspots caused by **^{14}C exudates** released from roots into the soil and ^{14}C activity **of the roots themselves**. In many cases (Holz et al., 2018; Pausch and Kuzyakov, 2011), ^{14}C activity in living or dry roots corresponds to the highest grey value (top values on the 255 gray scale) of 8-bit images and creates a peak on the right border of the 255 scale. Therefore, if the research question involves determining root exudation hotspots, the activity of roots alone should be separated beforehand by masking. Otherwise, exudate hotspots may be segmented with the background as well.

Importantly, all these (and probably some other) limitations are the same for all approaches (Mean+2SD, Mean+3SD, Top-25%, as well as the 17 approaches implemented in ImageJ) and mainly reflect the nature of the hotspots and the quality of the original images. Further quality improvements of imaging analysis (Baveye et al., 2010) and ongoing development of thresholding approaches (Iassonov et al., 2009; Sezgin and Sankur, 2004) are necessary for more objective conclusions on soil hotspot areas, localization and other characteristics.

4.4. Relevance and advantages of statistical approaches

1) The suggested Mean+2SD thresholding approach helps to avoid subjective biases in hotspot determination for various parameters such as enzyme activities, rhizodeposition, soil pH and nutrient concentrations. Thresholding based on intensity may result in multi-fold higher average activities for β-glucosidase, chitinase and acid phosphatase hotspots in comparison to non-hotspots (Heitkötter and Marschner, 2018), but much smaller hotspot areas (Top-25%, Figs. 2 and 3). The enzyme activities in hotspots and background differed greatly (up to 7 times) because the hotspot segmentation was done by a non-statistical approach and is biased on a few points with maximal intensity. Moreover, using the Mean+2SD approach yields hotspot images that are visually similar to the originals, but with a distinct and completely black background (Figs. 2-4). In contrast, the very small hotspot areas thresholded using the Top-25% approach yielded subtle (almost "background" covered) hotspot images for enzyme activity (Fig. 2) and lower contrast images for ^{14}C activity (Fig. 3 and 4). Thus, the Mean+2SD thresholding approach enables localizing i) microbial hotspots along the whole root system for enzyme activity (Fig. 2), ii) ^{14}C allocation hotspots in smaller roots (Fig. 3), and iii) glyphosate accumulation hotspots in the seedling and primary root as opposed to only in leaves for the Top-25% approach (Fig. 4).

2) The Mean+2SD and Mean+3SD approaches are much more reliable than Top-25% for microbial (e.g. enzyme activity) hotspot determinations in temporal sequences of images. The thresholding background with contrasting enzyme activity at successive time points can highlight hotspot development, the "time-specific" hotspots and, thus, their lifetime. Accordingly, the set thresholding value for activity may correspond to hotspots at one time point and to the hottest spots at another one (hot moment); the reverse situation is also possible. The challenge to define hotspots at any time, however, is solved by background thresholding. Mean+2SD and Mean+3SD are the universal approaches to overcome such temporal changes of activity and to qualitatively determine hotspot dynamics.

3) The background thresholding approach enables defining the hotspots for various properties with the same statistical approach (enzyme activities, ^{14}C in root exudates, water content, soil pH, soil CO_2 and O_2, nutrient concentrations, etc.). Mean+2SD separates hotspots from the background regardless of their location within a range of low, medium or higher activities. Thereafter, hotspot images can be co-localized and conclusions can be drawn about their spatial co-occurrence.

4) These statistical approaches enable identifying hotspots with various levels of microbial activities or substance concentrations in soil. Both Mean+2SD and Mean+3SD (Razavi et al., 2019) can be used to identify hotspots with high and very high activities. The Mean+3SD approach will highlight the areas with 0.15% highest activities and cut off the "background" with 99.85% lowest activities. Nonetheless, the Mean+3SD approach should be applied with caution, especially for microbial hotspots in the rhizosphere. It might disregard the values along less active rhizosphere parts, and the rhizosphere zones as a microbial hotspot will be incomplete (Figs. 2 and 3). That approach yielded 1.3-2.2 times smaller hotspot areas than Mean+2SD. Hotspots in the rhizosphere were lost along the smaller roots (Figs. 2 and 3) by Mean+3SD. Therefore, that thresholding approach is more appropriate for the highest microbial or ^{14}C activity hotspots and used with discretion for rhizosphere studies.

5) Last but not least, the Mean+1SD/Mean+2SD/ Mean+3SD approaches are very simple and based on a clear principle. The parameters of normal distribution can be fitted easily by free and commonly used imaging software and statistical tools (R, ImageJ, etc.). No special software and tools, nor deep involvement with complex thresholding approaches, are necessary.

5. Conclusions

Although microbial hotspots are among the hot topics in soil science, and various imaging techniques help visualize and localize them, statistical approaches to identify the hotspots have not been used. For the first time, we propose simple statistical approaches to separate hotspots from soil background activities on 2-D images. Our approaches are based on the probability of image areas with intensities higher than mean + 2 standard deviations (Mean+2SD) or + 3 standard deviations (Mean+3SD) of a normal distribution. The Mean+2SD or Mean+3SD approaches include: 1) splitting the greyscale histogram of the image into two histograms with normal distribution of greyscale values; 2) identifying the greyscale range corresponding to the hotspots; and 3) hotspot mapping on the original image. This methodology helps to avoid under- or overestimation and bias in images of lower quality, is applicable to time series experiments, and can couple imaging methods of various parameters.

Acknowledgements

We are very thankful to Sandra Spielvogel for her valuable comments that greatly improved the manuscript. We gratefully acknowledge the Interfaculty Research Cooperation (IRC) “One Health” at University of Bern, Sub-Project 4. Support for this research was provided in part by the USDA NIFA Program (Award # 2019-67019-29361), by the NSF LTER Program (DEB 1027253) at the Kellogg Biological Station, by USDA NC1187 project, by the Great Lakes Bioenergy Research Center, U.S. Department of Energy, Office of Science, Office of Biological and Environmental Research under Award Number DE-SC0018409, and by Michigan State University AgBioResearch. Contribution of Yakov Kuzyakov was supported by the Russian Science Foundation (project No. 18-14-00362). We would like to thank the two anonymous reviewers for their suggestions and comments.

References

Alcántara-de la Cruz, R., Fernández-Moreno, P.T., Ozuna, C. V., Rojano-Delgado, A.M., Cruz-Hipolito, H.E., Domínguez-Valenzuela, J.A., Barro, F., de Prado, R., 2016. Target and non-target site mechanisms developed by glyphosate-resistant hairy beggarticks (Bidens pilosa L.) populations from Mexico. Front. Plant Sci. 7, 1–12. https://doi.org/10.3389/fpls.2016.01492

Aslantas, A., Emre, D., Çakiroğlu, M., 2017. Comparison of segmentation algorithms for detection of hotspots in bone scintigraphy images and effects on CAD systems. Biomed. Res. 28, 676–683.

Baveye, P.C., Laba, M., Otten, W., Bouckaert, L., Dello Sterpaio, P., Goswami, R.R., Grinev, D., Houston, A., Hu, Y., Liu, J., Mooney, S., Pajor, R., Sleutel, S., Tarquis, A., Wang, W., Wei, Q., Sezgin, M., 2010. Observer-dependent variability of the thresholding step in the quantitative analysis of soil images and X-ray microtomography data. Geoderma 157, 51–63. https://doi.org/10.1016/j.geoderma.2010.03.015

Benaglia, T., Chauveau, D., Hunter, D.R., Young, D.S., 2009. Mixtools: An R package for analyzing finite mixture models. J. Stat. Softw. 32, 1–29. https://doi.org/10.18637/jss.v032.i06

Bertrand, I., Grignon, N., Hinsinger, P., Souche, G., Jaillard, B., 2001. The use of secondary ion mass spectrometry coupled with image analysis to identify and locate chemical elements in soil minerals: The example of phosphorus. Scanning 23, 279–291. https://doi.org/10.1002/sca.4950230409

Carminati, A., Moradi, A.B., Vetterlein, D., Vontobel, P., Lehmann, E., Weller, U., Vogel, H.J., Oswald, S.E., 2010. Dynamics of soil water content in the rhizosphere. Plant Soil 332, 163–176. https://doi.org/10.1007/s11104-010-0283-8

Chu, A., Cui, J., Dinov, I.D., 2009. SOCR Analyses: Implementation and Demonstration of a New Graphical Statistics Educational Toolkit . J. Stat. Softw. 30, 1–19. https://doi.org/10.18637/jss.v030.i03

Dinov, I.D., 2011. Neurological imaging: Statistics behind the pictures. Imaging Med. https://doi.org/10.2217/iim.11.37

Gao, W., Schlüter, S., Blaser, S.R.G.A., Shen, J., Vetterlein, D., 2019. A shape-based method for automatic and rapid segmentation of roots in soil from X-ray computed tomography images: Rootine. Plant Soil 441, 643–655. https://doi.org/10.1007/s11104-

019-04053-6

Ge, T., Wei, X., Razavi, B.S., Zhu, Z., Hu, Y., Kuzyakov, Y., Jones, D.L., Wu, J., 2017. Stability and dynamics of enzyme activity patterns in the rice rhizosphere: Effects of plant growth and temperature. Soil Biol. Biochem. 113, 108–115. https://doi.org/10.1016/j.soilbio.2017.06.005

Guber, A., Kravchenko, A., Razavi, B.S., Uteau, D., Peth, S., Blagodatskaya, E., Kuzyakov, Y., 2018. Quantitative soil zymography: Mechanisms, processes of substrate and enzyme diffusion in porous media. Soil Biol. Biochem. 127, 156–167. https://doi.org/10.1016/j.soilbio.2018.09.030

Handschuh, S., Baeumler, N., Schwaha, T., Ruthensteiner, B., 2013. A correlative approach for combining microCT, light and transmission electron microscopy in a single 3D scenario. Front. Zool. 10, 1. https://doi.org/10.1186/1742-9994-10-44

Heitkötter, J., Marschner, B., 2018. Soil zymography as a powerful tool for exploring hotspots and substrate limitation in undisturbed subsoil. Soil Biol. Biochem. 124, 210–217. https://doi.org/10.1016/j.soilbio.2018.06.021

Hoang, D.T.T., Razavi, B.S., Kuzyakov, Y., Blagodatskaya, E., 2016. Earthworm burrows: Kinetics and spatial distribution of enzymes of C-, N- and P- cycles. Soil Biol. Biochem. 99, 94–103. https://doi.org/10.1016/J.SOILBIO.2016.04.021

Holz, M., Zarebanadkouki, M., Carminati, A., Kuzyakov, Y., 2019. Visualization and quantification of root exudation using 14C imaging: challenges and uncertainties. Plant Soil 437, 473–485. https://doi.org/10.1007/s11104-019-03956-8

Holz, M., Zarebanadkouki, M., Kuzyakov, Y., Pausch, J., Carminati, A., 2018. Root hairs increase rhizosphere extension and carbon input to soil. Ann. Bot. 121, 61–69. https://doi.org/10.1093/aob/mcx127

Huang, L.K., Wang, M.J.J., 1995. Image thresholding by minimizing the measures of fuzziness. Pattern Recognit. 28, 41–51. https://doi.org/10.1016/0031-3203(94)E0043-K

Hussain, M., Chen, D., Cheng, A., Wei, H., Stanley, D., 2013. Change detection from remotely sensed images: From pixel-based to object-based approaches. ISPRS J. Photogramm. Remote Sens. https://doi.org/10.1016/j.isprsjprs.2013.03.006

Iassonov, P., Gebrenegus, T., Tuller, M., 2009. Segmentation of X-ray computed tomography images of porous materials: A crucial step for characterization and quantitative analysis of pore structures. Water Resour. Res. 45, 1–12. https://doi.org/10.1029/2009WR008087

Kravchenko, A., Chun, H.C., Mazer, M., Wang, W., Rose, J.B., Smucker, A., Rivers, M., 2013. Relationships between intra-aggregate pore structures and distributions of Escherichia coli within soil macro-aggregates. Appl. Soil Ecol. 63, 134–142. https://doi.org/10.1016/j.apsoil.2012.10.001

Kravchenko, A.N., Guber, A.K., Razavi, B.S., Koestel, J., Blagodatskaya, E. V, Kuzyakov, Y., 2019a. Spatial patterns of extracellular enzymes: Combining X-ray computed micro-tomography and 2D zymography. Soil Biol. Biochem. 135, 411–419. https://doi.org/10.1016/j.soilbio.2019.06.002

Kravchenko, A.N., Guber, A.K., Razavi, B.S., Koestel, J., Quigley, M.Y., Robertson, G.P., Kuzyakov, Y., 2019b. Microbial spatial footprint as a driver of soil carbon stabilization. Nat. Commun. 10, 3121. https://doi.org/10.1038/s41467-019-11057-4

Kuzyakov, Y., Blagodatskaya, E., 2015. Microbial hotspots and hot moments in soil: Concept & review. Soil Biol. Biochem. 83, 184–199. https://doi.org/10.1016/j.soilbio.2015.01.025

Kuzyakov, Y., Razavi, B.S., 2019. Rhizosphere size and shape: Temporal dynamics and spatial stationarity. Soil Biol. Biochem. 135, 343–360. https://doi.org/10.1016/J.SOILBIO.2019.05.011

Landini, G., 2017. ImageJ , 1.16.5 [WWW Document].

Lee, S.U., Yoon Chung, S., Park, R.H., 1990. A comparative performance study of several global thresholding techniques for segmentation. Comput. Vision, Graph. Image

512 Process. 52, 171–190. https://doi.org/10.1016/0734-189X(90)90053-X
513 Liu, S., Razavi, B.S., Su, X., Maharjan, M., Zarebanadkouki, M., Blagodatskaya, E.,
514 Kuzyakov, Y., 2017. Spatio-temporal patterns of enzyme activities after manure
515 application reflect mechanisms of niche differentiation between plants and
516 microorganisms. Soil Biol. Biochem. 112, 100–109.
517 https://doi.org/10.1016/j.soilbio.2017.05.006
518 Logan, B.R., Geliazkova, M.P., Rowe, D.B., 2008. An evaluation of spatial thresholding
519 techniques in fMRI analysis. Hum. Brain Mapp. 29, 1379–1389.
520 https://doi.org/10.1002/hbm.20471
521 Lv, L., Liao, K., Zhou, Z., Zhu, Q., Shen, C., 2019. Determining hot moments/spots of
522 hillslope soil moisture variations based on high-resolution spatiotemporal soil moisture
523 data. Catena 173, 150–161. https://doi.org/10.1016/J.CATENA.2018.10.012
524 Ma, X., Razavi, B.S., Holz, M., Blagodatskaya, E., Kuzyakov, Y., 2017. Warming increases
525 hotspot areas of enzyme activity and shortens the duration of hot moments in the root-
526 detritusphere. Soil Biol. Biochem. 107, 226–233.
527 https://doi.org/10.1016/j.soilbio.2017.01.009
528 Matsuyama, E., Takahashi, N., Watanabe, H., Tsai, D., 2016. A Method of Using Information
529 Entropy of an Image as an Effective Feature for Com-puter-Aided Diagnostic
530 Applications. J. Biomed. Sci. Eng. 09, 315–322. https://doi.org/10.4236/jbise.2016.96026
531 Mortazavi, D., Z. Kouzani, A., Zadeh, H.S.-, 2012. A 3S Multi-level Thresholding Technique
532 for Intracranial Segmentation from Brain MRI Images. J. Bioeng. Biomed. Sci. 02.
533 https://doi.org/10.4172/2155-9538.1000109
534 Nandula, V.K., Vencill, W.K., 2015. Herbicide Absorption and Translocation in Plants using
535 Radioisotopes. Weed Sci. 63, 140–151. https://doi.org/10.1614/ws-d-13-00107.1
536 Nunan, N., Ritz, K., Crabb, D., Harris, K., Wu, K., Crawford, J.-W., Young, I.-M., 2001.
537 Quantification of the in situ distribution of soil bacteria by large-scale imaging of thin

sections of undisturbed soil. FEMS Microbiol. Ecol. 37 (1), 67-77. https://doi.org/10.1111/j.1574-6941.2001.tb00854.x

Nunan, N., Wu, K., Young, I.M., Crawford, J.W., Ritz, K., 2003. Spatial distribution of bacterial communities and their relationships with the micro-architecture of soil. FEMS Microbiol. Ecol. 44, 203–215. https://doi.org/10.1016/S0168-6496(03)00027-8

Nunan, N., Wu, K., Young, I.M., Crawford, J.W., Ritz, K., 2002. In situ spatial patterns of soil bacterial populations, mapped at multiple scales, in an arable soil. Microb. Ecol. 44, 296–305. https://doi.org/10.1007/s00248-002-2021-0

Oburger, E., Schmidt, H., 2016. New Methods To Unravel Rhizosphere Processes. Trends Plant Sci. 21, 243–255. https://doi.org/10.1016/j.tplants.2015.12.005

Otsu, N., 1979. A Threshold Selection Method from Gray-Level Histograms. IEEE Trans. Syst. Man. Cybern. 9, 62–66. https://doi.org/10.1109/TSMC.1979.4310076

Pausch, J., Kuzyakov, Y., 2011. Photoassimilate allocation and dynamics of hotspots in roots visualized by 14C phosphor imaging. J. Plant Nutr. Soil Sci. 174, 12–19. https://doi.org/10.1002/jpln.200900271

Pereira, F.C.M., Tayengwa, R., Alves, P.L.D.C.A., Peer, W.A., 2019. Phosphate Status Affects Phosphate Transporter Expression and Glyphosate Uptake and Transport in Grand Eucalyptus (Eucalyptus grandis). Weed Sci. 67, 29–40. https://doi.org/10.1017/wsc.2018.58

Polzer, C., Ness, S., Mohseni, M., Kellerer, T., Hilleringmann, M., Rädler, J., Hellerer, T., 2019. Correlative two-color two-photon (2C2P) excitation STED microscopy. Biomed. Opt. Express 10, 4516. https://doi.org/10.1364/boe.10.004516

Prewitt, J.M.S., Mendelsohn, M.L., 1966. The analysis of cell images. Ann. N. Y. Acad. Sci. 128, 1035–1053. https://doi.org/10.1111/j.1749-6632.1965.tb11715.x

Protz, R., Shipitalo, M.J., Mermut, A.R., Fox, C.A., 1987. Image analysis of soils - present and future. Geoderma 40, 115–125. https://doi.org/10.1016/0016-7061(87)90017-6

564 Qiu, Y., Fu, B., Wang, J., Chen, L., 2003. Spatiotemporal prediction of soil moisture content
565 using multiple-linear regression in a small catchment of the Loess Plateau, China.
566 Catena 54, 173–195. https://doi.org/10.1016/S0341-8162(03)00064-X
567 R Developement Core Team, 2014. R: a language and environment for statistical computing,
568 R Foundation for Statistical Computing.
569 Razavi, B.S., Hoang, D., Kuzyakov, Y., 2017. Visualization of Enzyme Activities in Earthworm
570 Biopores by In Situ Soil Zymography, in: Wilkesman, J., Kurz, L. (Eds.), Methods in
571 Molecular Biology, Methods in Molecular Biology. Springer New York, New York, NY, pp.
572 229–238. https://doi.org/10.1007/978-1-4939-7111-4
573 Razavi, B.S., Zarebanadkouki, M., Blagodatskaya, E., Kuzyakov, Y., 2016. Rhizosphere
574 shape of lentil and maize: Spatial distribution of enzyme activities. Soil Biol. Biochem.
575 79, 229–237. https://doi.org/10.1016/j.soilbio.2016.02.020
576 Razavi, B.S., Zhang, X., Bilyera, N., Guber, A., Zarebanadkouki, M., 2019. Soil zymography:
577 Simple and reliable? Review of current knowledge and optimization of the method.
578 Rhizosphere 11, 100161. https://doi.org/10.1016/J.RHISPH.2019.100161
579 Roose, T., Keyes, S.D., Daly, K.R., Carminati, A., Otten, W., Vetterlein, D., Peth, S., 2016.
580 Challenges in imaging and predictive modeling of rhizosphere processes. Plant Soil 407,
581 9–38. https://doi.org/10.1007/s11104-016-2872-7
582 Satapathy, S.C., Sri Madhava Raja, N., Rajinikanth, V., Ashour, A.S., Dey, N., 2018. Multi-
583 level image thresholding using Otsu and chaotic bat algorithm. Neural Comput. Appl. 29,
584 1285–1307. https://doi.org/10.1007/s00521-016-2645-5
585 Schindelin, J., Arganda-Carreras, I., Frise, E., Kaynig, V., Longair, M., Pietzsch, T., Preibisch,
586 S., Rueden, C., Saalfeld, S., Schmid, B., Tinevez, J.-Y., White, D.J., Hartenstein, V.,
587 Eliceiri, K., Tomancak, P., Cardona, A., 2012. Fiji: an open-source platform for
588 biological-image analysis. Nat. Methods 9, 676–682. https://doi.org/10.1038/nmeth.2019
589 Schlüter, S., Sheppard, A., Brown, K., Wildenschild, D., 2014. Image processing of

multiphase images obtained via X-ray microtomography: A review. Water Resour. Res. 50, 3615–3639. https://doi.org/10.1002/2014WR015256

Sezgin, M., Sankur, B., 2004. Survey over image thresholding techniques and quantitative performance evaluation. J. Electron. Imaging 13, 146–165. https://doi.org/10.1117/1.1631315

Spohn, M., Carminati, A., Kuzyakov, Y., 2013. Soil zymography - A novel in situ method for mapping distribution of enzyme activity in soil. Soil Biol. Biochem. 58, 275–280. https://doi.org/10.1016/j.soilbio.2012.12.004

Spohn, M., Kuzyakov, Y., 2014. Spatial and temporal dynamics of hotspots of enzyme activity in soil as affected by living and dead roots-a soil zymography analysis. Plant Soil 379, 67–77. https://doi.org/10.1007/s11104-014-2041-9

Steffens, M., Buddenbaum, H., 2013. Laboratory imaging spectroscopy of a stagnic Luvisol profile - High resolution soil characterisation, classification and mapping of elemental concentrations. Geoderma 195–196, 122–132. https://doi.org/10.1016/j.geoderma.2012.11.011

Steffens, M., Kohlpaintner, M., Buddenbaum, H., 2014. Fine spatial resolution mapping of soil organic matter quality in a Histosol profile. Eur. J. Soil Sci. 65, 827–839. https://doi.org/10.1111/ejss.12182

Tajima, R., Kato, Y., 2013. A quick method to estimate root length in each diameter class using Freeware Imagej. Plant Prod. Sci. 16, 9–11. https://doi.org/10.1626/pps.16.9

Tajima, R., Kato, Y., 2011. Comparison of threshold algorithms for automatic image processing of rice roots using freeware ImageJ. F. Crop. Res. 121, 460–463. https://doi.org/10.1016/j.fcr.2011.01.015

Werner, F., Mueller, C.W., Thieme, J., Gianoncelli, A., Rivard, C., Höschen, C., Prietzel, J., 2017. Micro-scale heterogeneity of soil phosphorus depends on soil substrate and depth. Sci. Rep. 7, 1–9. https://doi.org/10.1038/s41598-017-03537-8

Weszka, J.S., Rosenfeld, A., 1978. Threshold Evaluation Techniques. IEEE Trans. Syst. Man. Cybern. 8, 622–629. https://doi.org/10.1109/TSMC.1978.4310038

Zack, G.W., Rogers, W.E., Latt, S.A., 1977. Automatic measurement of sister chromatid exchange frequency. J. Histochem. Cytochem. 25, 741–753. https://doi.org/10.1177/25.7.70454

Zhang, X., Dippold, M.A., Kuzyakov, Y., Razavi, B.S., 2019. Spatial pattern of enzyme activities depends on root exudate composition. Soil Biol. Biochem. 133, 83–93. https://doi.org/10.1016/J.SOILBIO.2019.02.010

Zhu, Q., Zhou, Z., Duncan, E.W., Lv, L., Liao, K., Feng, H., 2017. Integrating real-time and manual monitored data to predict hillslope soil moisture dynamics with high spatio-temporal resolution using linear and non-linear models. J. Hydrol. 545, 1–11. https://doi.org/10.1016/J.JHYDROL.2016.12.014

629 **TABLES**

630 **Table 1** Approaches to hotspot determination of selected soil parameters in 2-D images

Parameter/ method	Approach	Reference
Enzyme activity/ Soil zymography	Top-25% of grey values	Ma et al., 2017
	>50% of mean values	Heitkötter and Marschner, 2018
	>20% of mean grey values	Zhang et al., 2019
	Above of average grey value (>70%)	Liu et al., 2017
	ANOVA to confirm the boundaries by 5 adjusted pixels	Hoang et al., 2016, Ge et al., 2017
	Percentage of segmented areas (thresholded by enzyme activity levels)	Spohn and Kuzyakov, 2014
Soil moisture content/ mapping	Variation indexes	Lv et al., 2019
	Multiple-linear regression	Qiu et al., 2003
	Linear and non-liner models	Zhu et al., 2017
NanoSIMS Light and fluorescent microscopy, SIMs and NanoSIMs	Thresholding by size	Xiao et al., 2016
	Correlative imaging	Handschuh et al., 2013; Polzer et al., 2019

631

632

633 **Table 2.** Comparison of hotspot areas on three images of activity distribution in soils or plants
634 calculated by Mean+2SD, Mean+3SD and Top-25% approaches.

Method	Parameter	Hotspots area, %			Hotspot area increase compared to Top-25%, times	
		Top-25%	Mean +2SD	Mean +3SD	Mean +2SD	Mean +3SD
Soil zymography (Fig. 2)	leucine aminopeptidase activity	0.2	12	7.1	60	36
^{14}C imaging (Fig. 3 and 4)	^{14}C in root exudates and roots	5.8	23.2	17.1	4	3
	Glyphosate (^{14}C) in plant	0.33	1.52	0.87	4.6	2.6

635
636

637 **FIGURES**

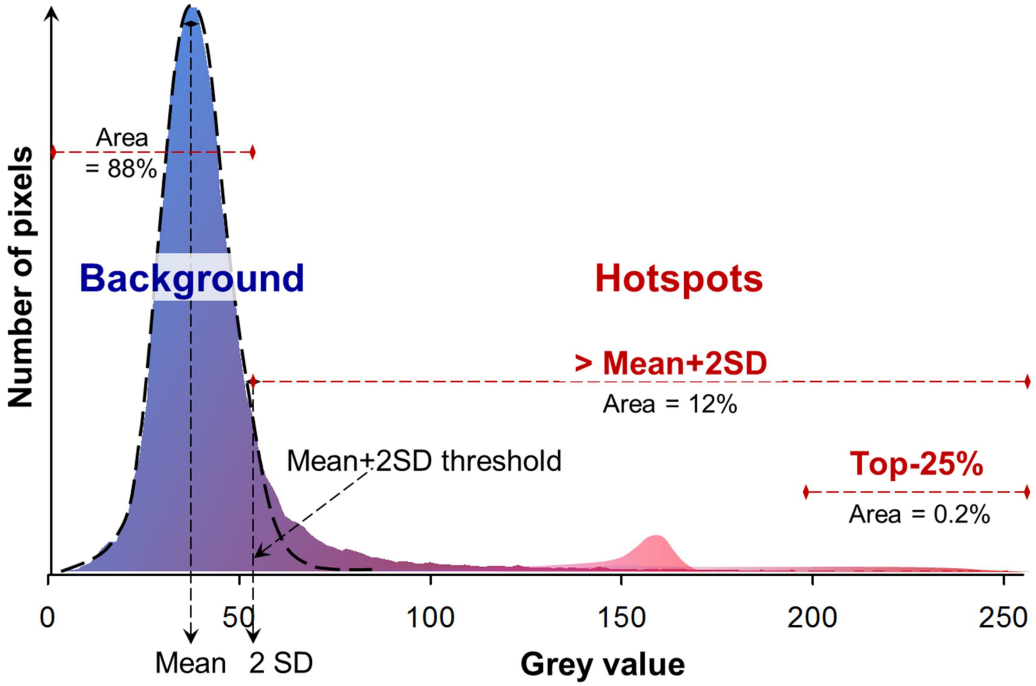

638

639 **Fig. 1.** An example of the grey value distribution (from 0 to 255) for leucine aminopeptidase
640 activity in soil (data extracted from the 8-bit image in Fig. 6b in Razavi et al., 2017). The
641 dashed curve reflects the normal distribution of the grey values of the soil background for
642 enzyme activity with its mean + 2 standard deviations (presented as vertical dashed lines).
643 The hotspot area (S) thresholded by the Mean+2SD approach corresponds to 12% of the
644 whole image. Because the Top-25% approach is strongly biased by the highest grey value
645 (here 255), only 0.2% of the total area are highlighted as hotspots.

646

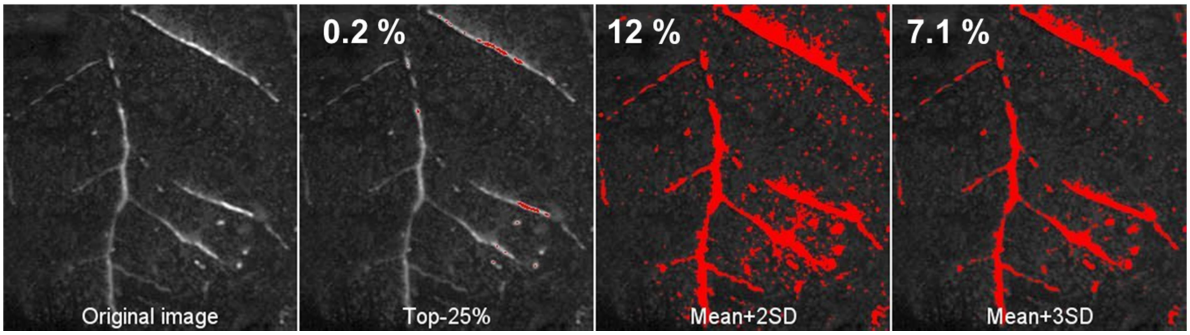

Fig. 2. Original soil zymograms of leucine aminopeptidase (Razavi et al., 2017) and hotspots (red) identified using Top-25%, Mean+2SD and Mean+3SD approaches (compare Fig. 1). Numbers on top left show the percentage of the total image area belonged to the hotspots.

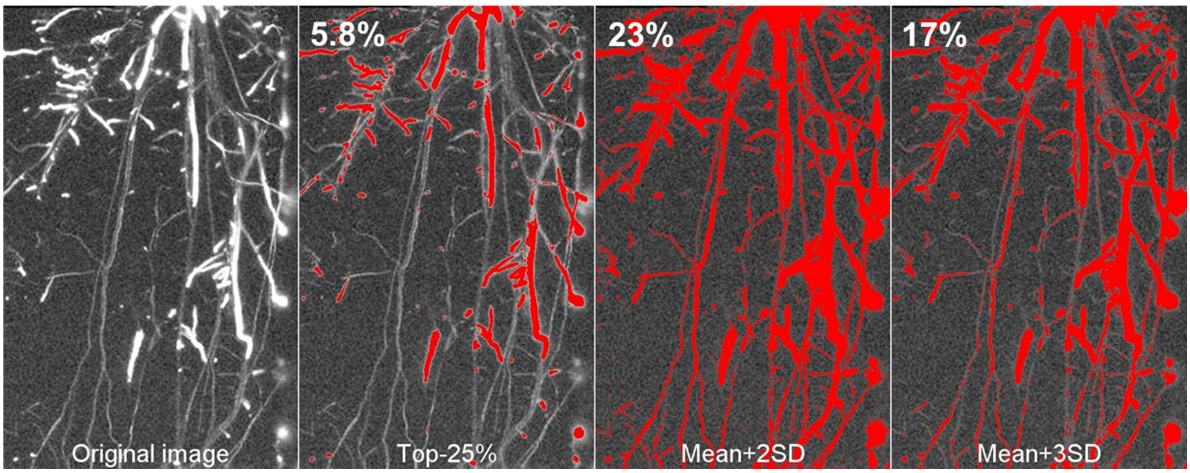

Fig. 3. Original and binarized images of roots and exudates in soil after labeling the plants with $^{14}CO_2$ (Holz et al., 2018). The hotspots (red) were identified using Top-25%, Mean+2SD and Mean+3SD approaches. Numbers on top left show the percentage of the total image area belonged to the hotspots.

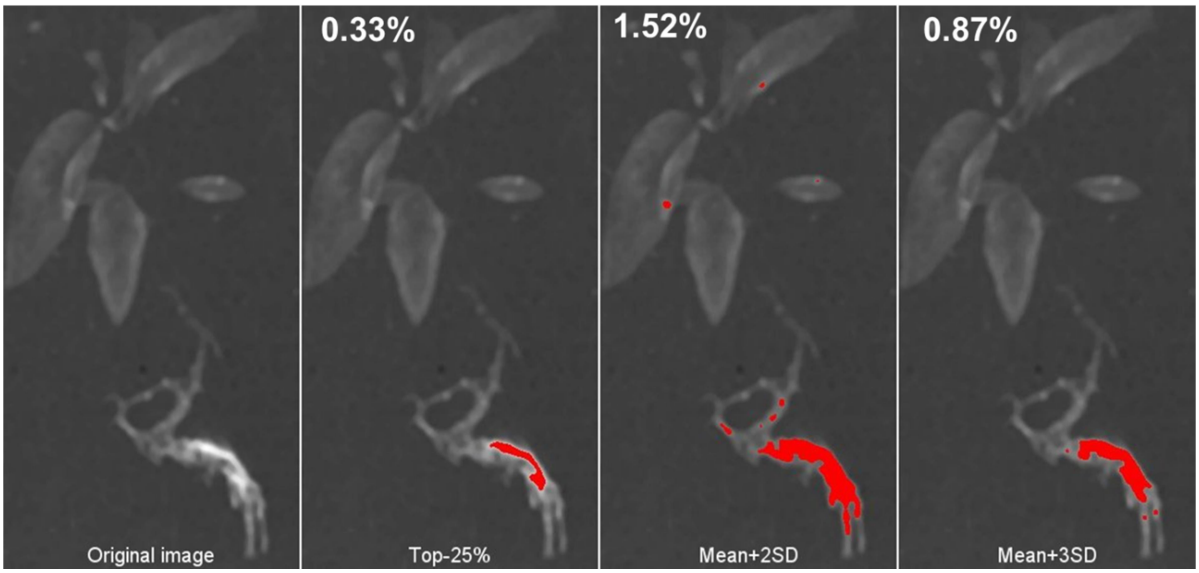

Fig. 4. Original and binarized images of ^{14}C-labeled glyphosate in plants (Fig 5 D, Pereira et al., 2019). The hotspots (red) were identified using Top-25%, Mean+2SD and Mean+3SD approaches. Numbers on top left show the percentage of the total image area belonged to the hotspots.

661

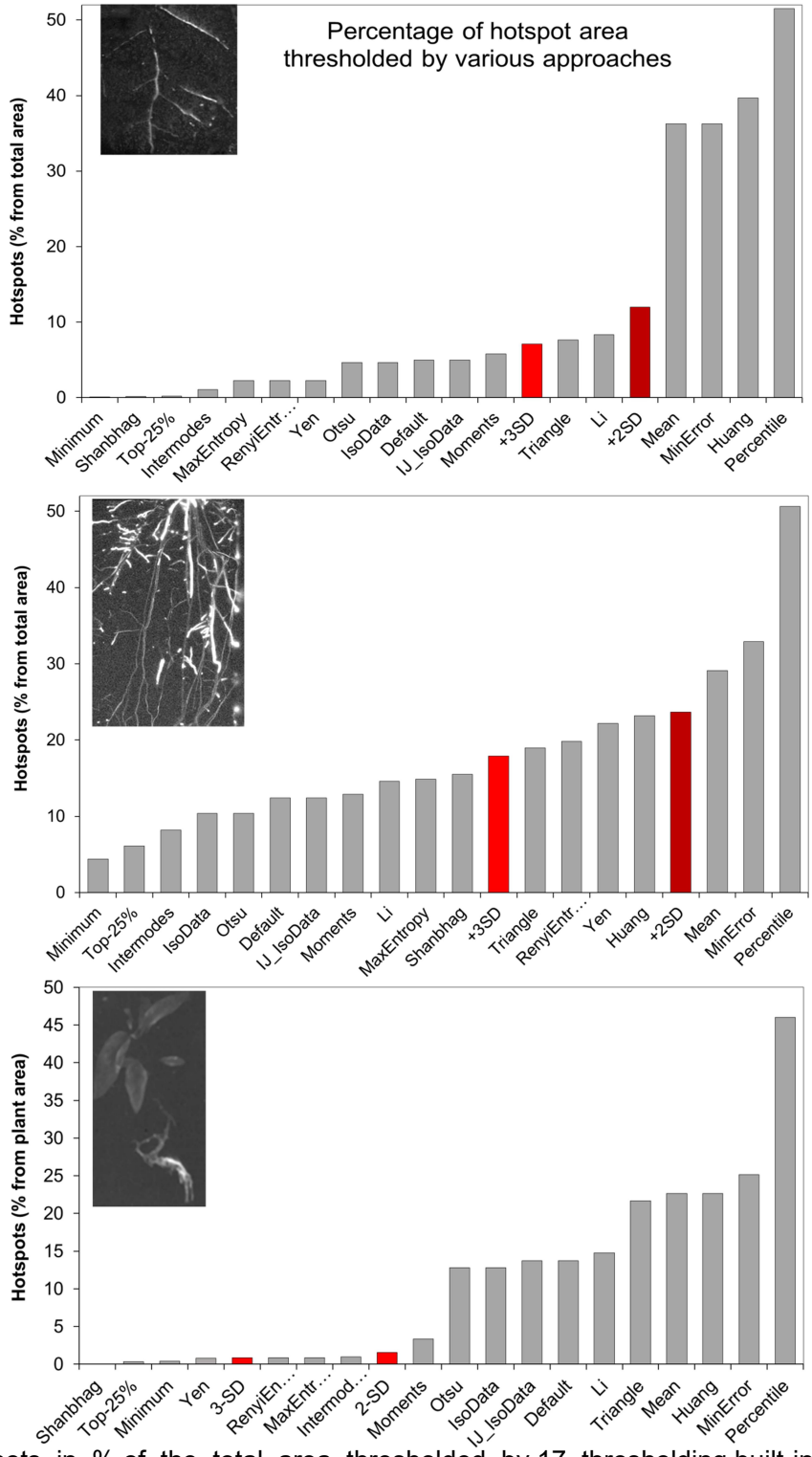

663

665

Fig. 5. Hotspots in % of the total area thresholded by 17 thresholding built-in methods in ImageJ and Mean+2SD, Mean+3SD or Top-25% for three test images: a) soil zymogram for leucine aminopeptidase (Razavi et al., 2017); b) ^{14}C image for $^{14}CO_2$-labeled root and exudates in soil and c) ^{14}C image of ^{14}C-labeled glyphosate in plants (Pereira et al., 2019).

669

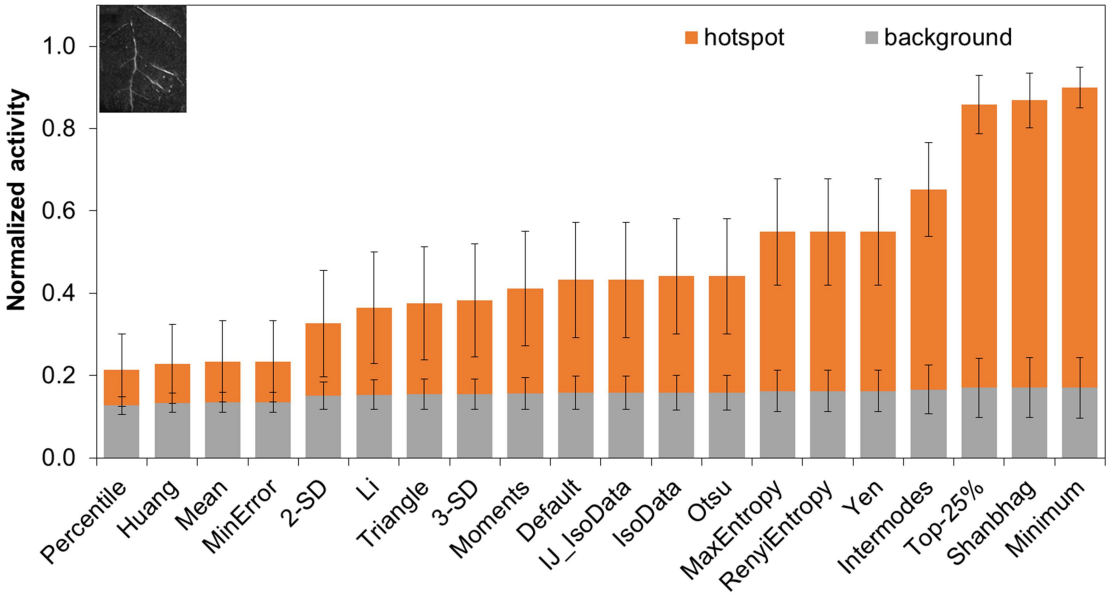

670 a)

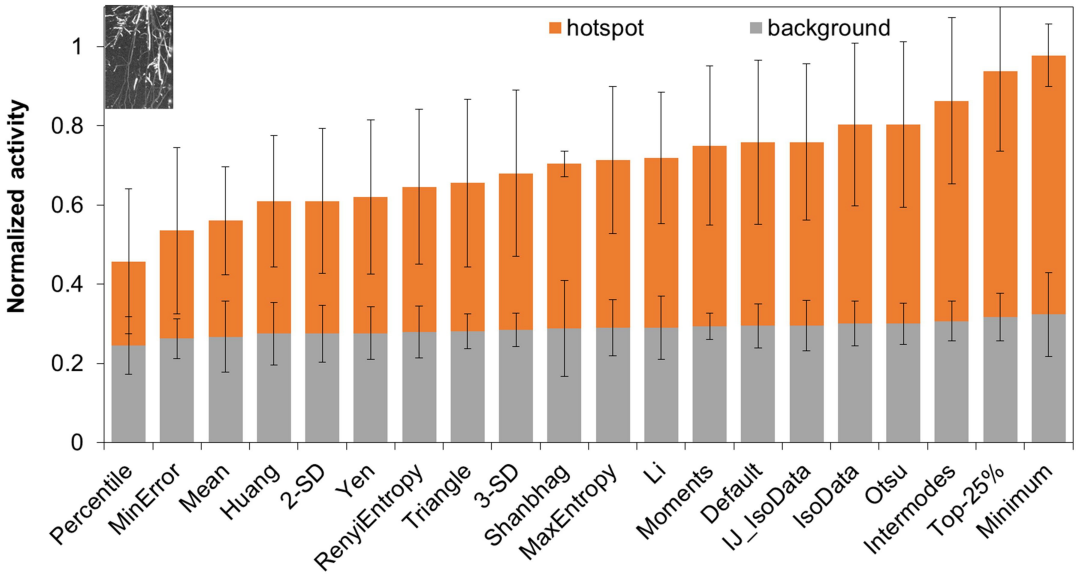

671 b)

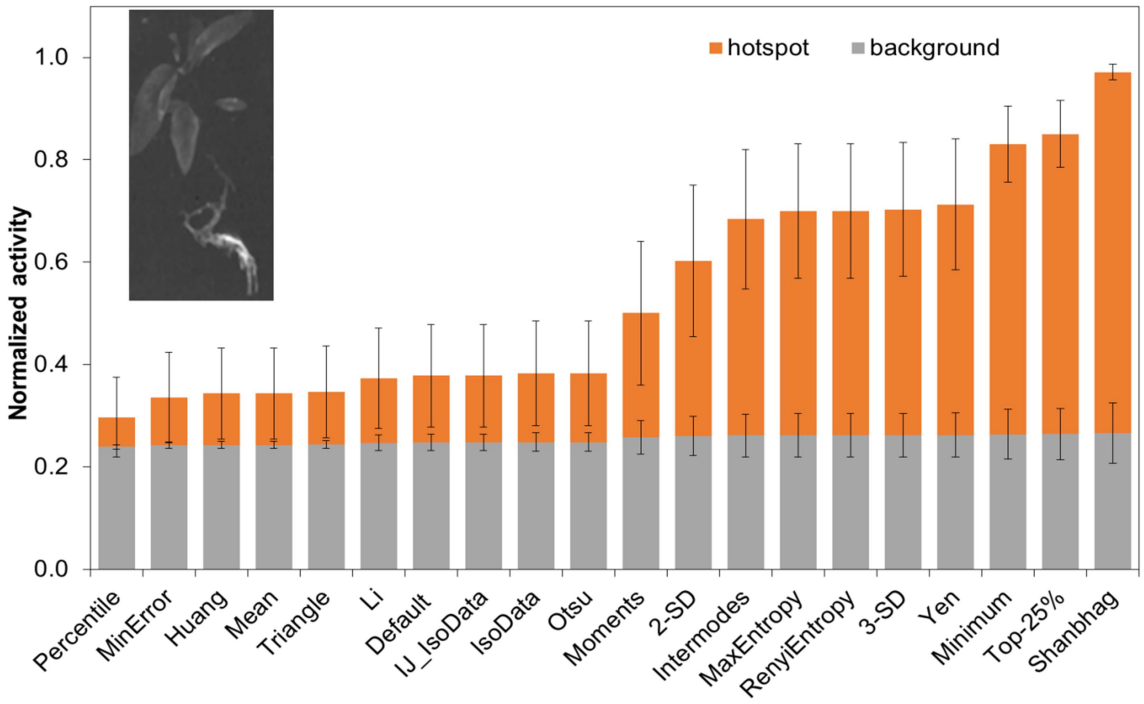

c)

Fig. 6. Normalized grey value activities for mean and standard deviation values for background and hotspots separated by 17 thresholding built-in methods in ImageJ and Mean+2SD, Mean+3SD or Top-25% for three test images: a) soil zymogram for leucine aminopeptidase (Razavi et al., 2017); b) ^{14}C image for $^{14}CO_2$-labeled root and exudates in soil (Holz et al., 2018) and c) ^{14}C image of ^{14}C-labeled glyphosate in plants (Pereira et al., 2019).

Supplementary Materials

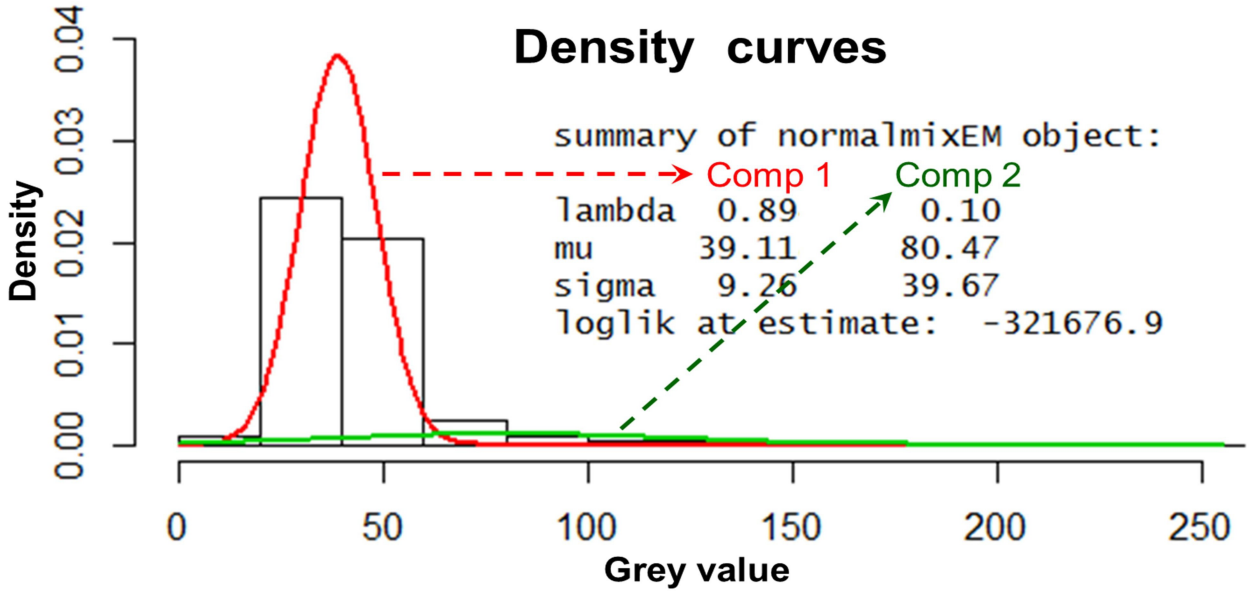

Figure S1. An example of the original grey value distribution (bars) for leucine aminopeptidase activity in soil (data extracted from the 8-bit image in Fig. 6b in Razavi et al., 2017) and two fitted normal distributions using the normalmixEM function in R. Red and green lines denote comp 1 and comp 2 distributions in the summary table. Red (comp 1) normal distribution covers (lambda (λ)) 89% of the values, while green covers only 11%. Mean values (mu (μ)) and SD (sigma (σ)) were 39 and 81, and 9 and 40 for red and green distribution, respectively.

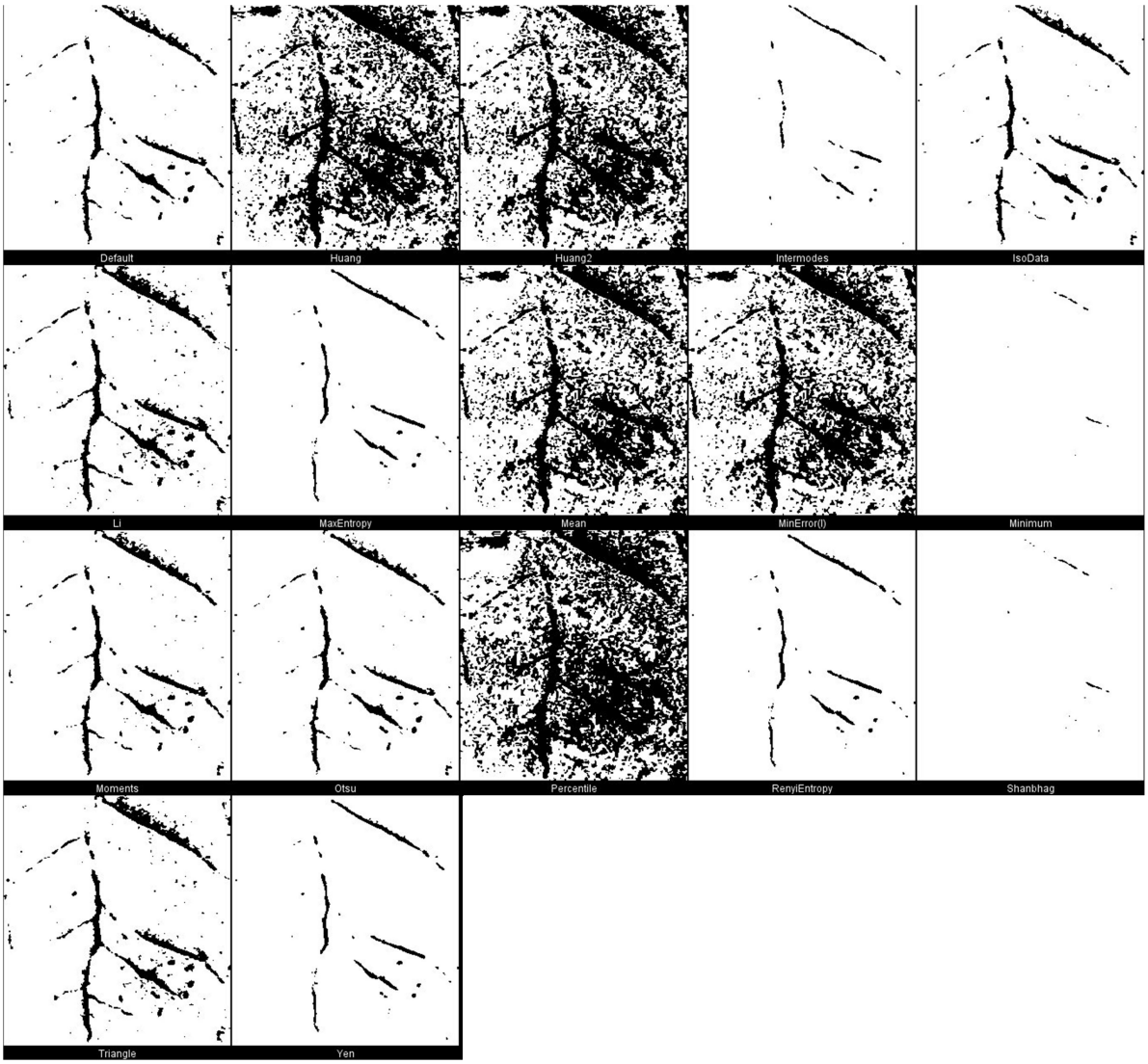

688

689

690 **Figure S2.** Montage image with results from all built-in thresholding methods in ImageJ
691 (Schindelin et al., 2012) applied to the soil zymogram for leucine aminopeptidase (Razavi et
692 al., 2017).

693 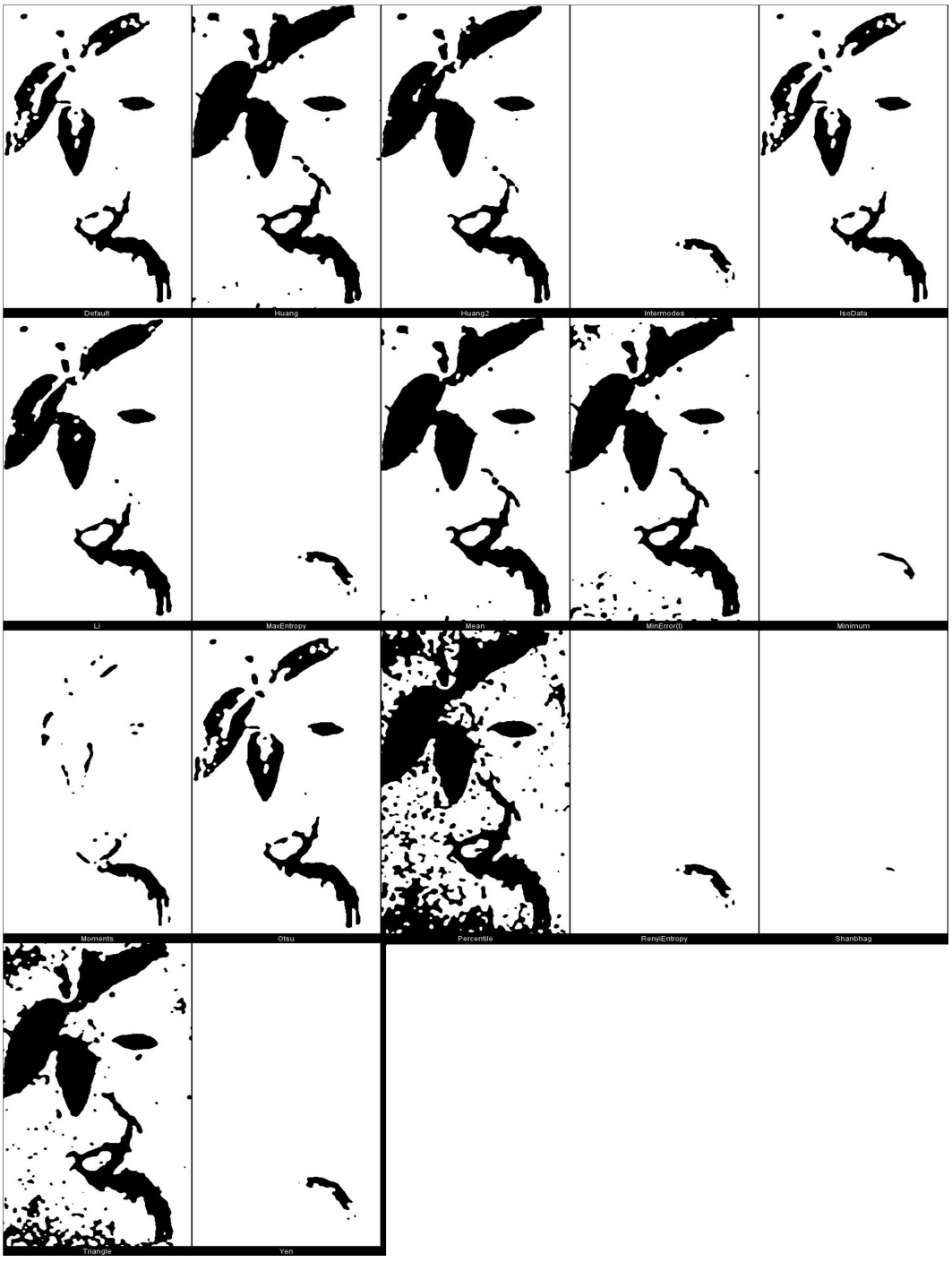

694 **Figure S3.** Montage image with results from all built-in thresholding methods in ImageJ
695 (Schindelin et al., 2012) applied to a ^{14}C image of ^{14}C-labeled glyphosate in plants (Pereira et
696 al., 2019).

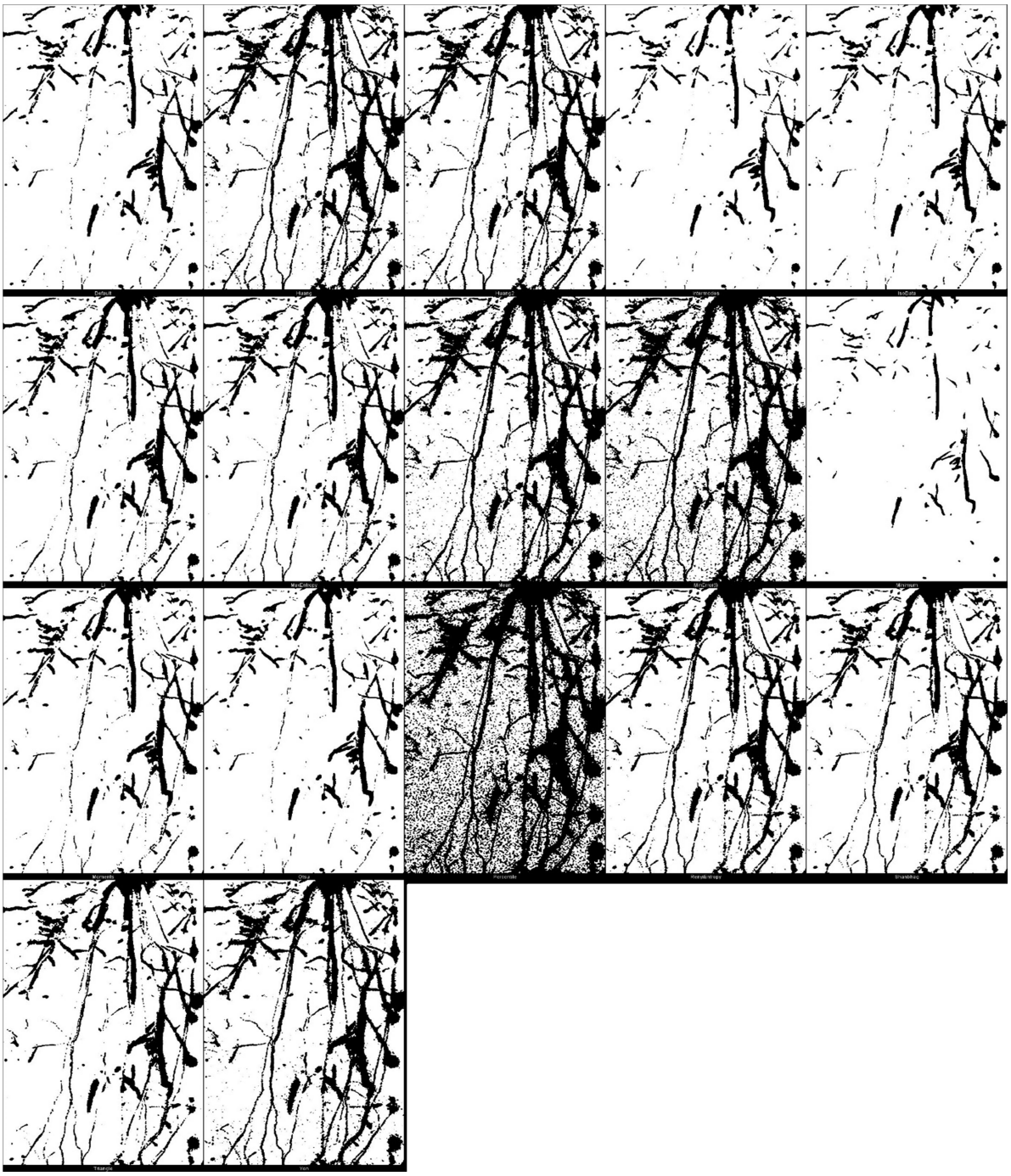

Figure S4. Montage image with results from all built-in thresholding methods in ImageJ (Schindelin et al., 2012) applied to a ^{14}C image for $^{14}CO_2$-labeled roots and exudates in soil (Holz et al., 2018).

Table S1. Results of two-samples t-Test for hotspot mean values between statistical approaches (Mean+2/3SD) and standard methods in ImageJ and Top-25%

Method	^{14}C image for $^{14}CO_2$-labeled root and exudates in soil (Holz et al., 2018)	Soil zymogram for leucine aminopeptidase (Razavi et al., 2017)			^{14}C image of ^{14}C-labeled glyphosate in plants (Pereira et al., 2019)	
	p-values					
	3SD	2SD	3SD	2SD	2SD	3SD
Default	0	0	1.92E-68	0	0	0
Huang	0	**1**	0	0	0	0
Intermodes	0	0	0	0	0	0
IsoData	0	0	1.94E-91	0	0	0
IJ_IsoData	0	0	1.92E-68	0	0	0
Li	8.89E-226	0	1.42E-12	7.83E-74	0	0
MaxEntropy	4.38E-175	0	0	0	0	**0.652**
Mean	0	0	0	0	0	0
MinError	0	0	0	0	0	0
Minimum	0	0	1.7E-279	0	0	0
Moments	0	0	5.56E-27	2.4E-269	0	0
Otsu	0	0	1.94E-91	0	0	0
Percentile	0	0	0	0	0	0
RenyiEntropy	8.87E-196	9.6E-241	0	0	0	**0.652**
Shanbhag	4.52E-91	0	0	0	0	0
Triangle	1.94E-99	0	**0.008838**	2.62E-112	0	0
Yen	0	2.97E-22	0	0	0	**0.148**
Top-25%	0	0	0	0	0	0

Example of script for distribution fitting of distribution parameters in R

```
install.packages("mixtools")
library(mixtools)
setwd("D:/Research/2019/Hot spot approach/Black and white/data for R")
Zymo1<-read.table('Zymo-leu.txt', header=T)
head(Zymo1)
value<-Zymo1$value
Amount<-Zymo1$amount
i<-seq(1,256, by=1)
#test normal distributions
vec<-rep(x=value[i], times = Amount[i])
mod <- normalmixEM(vec) #test normal distribution
plot(mod,which=2)
summary(mod)
```